Interpretation of magnetic anomalies using the horizontal gradient analytic signal

Nasreddine Bournas and Haydar Aziz Baker
Département de Géophysique, Faculté des Sciences de la Terre, USTHB, El-Alia, Bab Ezzouar, Alger, Algeria

Abstract
In recent years the analytic signal method has been of great utility in the interpretation of potential field data. The amplitude of the 3D analytic signal of magnetic data yields information on the location of the edges of the sources in both the horizontal and vertical dimensions, with the main advantage that the magnetic field and magnetic source parameters need not be known or assumed. Accurate detection of source body coordinates is becoming the main goal for interpreters and therefore enhanced techniques are acquiring an increasing revival in data interpretation. This paper presents a high-resolution approach for detecting source boundaries. These boundaries can be determined from the maxima of the analytic signal computed from the horizontal gradient of the field, defined here as a vector, the components of which are the analytic signals of x- and y-horizontal derivatives, respectively. Synthetic examples have shown the high resolving power of the proposed technique. This approach has also given very good results when applied to real data.

Key words *horizontal gradient – analytic signal – horizontal derivative – vertical derivative – interpretation – aeromagnetic anomaly – magnetic anomaly*

1. Introduction

One of the most important steps in the interpretation of the potential field data is to provide information on the horizontal location of the causative sources and their depths. Since the 1970s, several methods have been developed for the determination of the depth, geometry and density or magnetization of the potential sources: Spector and Grant (1970) developed the spectral method for computing the average depth of a set of sources. Their approach was based on the inspection and analysis of the slope of the power spectrum. Thompson (1982) proposed a method based on the equation of homogeneity of Euler applied to 2D profiles, which was later generalized by Reid *et al.* (1990) for 3D structures. The Euler deconvolution allows the location of the sources to be determined, and can be applied to gravity data as well as magnetic data. However, the degree of confidence of the solution depends on the correct choice of the structural index parameter. Cordell and Grauch (1985) suggested a method for the location of the horizontal extents of the sources from the maxima of the horizontal gradient of the pseudogravity computed from the magnetic anomalies. This method was automated by Blakely and Simpson (1986) and applied to the isostatic residual anomalies of the U.S.A. Nabighian (1972, 1974, 1984) extensively described the principles of the analytic signal method for the location of the 2D sources. In 1992, Roest *et al.*

Mailing address: Dr. Nasreddine Bournas, Cité Ibn Khaldoun, Bat. 51 B n. 9, Boumerdes 35000, Algeria; e-mail: n_bournas@yahoo.com

generalized the utilization of the analytic signal method for the location of the 3D sources. This method has recently become very popular among geophysicists, thanks to a number of advantages. Contrary to the gravity case, in which anomalies are generally located above the sources that produce them, the magnetic anomalies observed in the regions of low and middle latitudes show a polarity that complicates their interpretation. Such a shape of the magnetic anomalies is caused by the inclination of the induced field vector and/or the magnetization vector. To counter this 'skewness', Baranov (1957) introduced a transformation called reduction to the pole that allows the repositioning of the magnetic anomalies above the causative sources. This method, like most of the other techniques of analysis, requires the knowledge of the angles of inclination and declination of the inducing field vector and the magnetization vector. However, an important characteristic of the analytic signal method is that the amplitude of the analytic signal, for a thin two-dimensional body (dyke), is independent of the orientation of the induced field vector and that of the magnetization vector and it has a bell-shaped symmetric curve (the envelope of energy of a signal) located directly above the source (Roest *et al.*, 1992).

However, in the case of a thick body (thick dyke) or prismatic body (cylinder), when the horizontal dimensions exceed the depth to top, the inferred outlines of source boundaries from the maxima of the amplitude of analytic signal, as defined by Roest *et al.* (1992), seem to be insufficiently accurate because of the interference effects of the body extents. To improve the boundaries detection resolution, Marson and Kingele (1993) showed that the application of the analytic signal from the vertical gradient of gravity data yields the best results for locating density contrasts. More recently, Hsu *et al.* (1996) developed an enhanced analytic signal applied to the second order vertical derivative of potential-field anomalies. Their technique has provided a better visualization of outlines of shallow magnetic source bodies. The enhanced analytic signal, based on the *i*th order vertical derivative, was adopted as an automatic interpretation tool (Debeglia and Corpel, 1997, Hsu *et al.*, 1998). But, the major inconvenience of using high order vertical derivatives is due to the amplification of high frequency noise and the attenuation of deep source effects.

Recently, Fedi and Florio (2001) presented the enhanced horizontal method (EHD) for locating source boundaries. In their method they used the horizontal derivative of the sum of vertical derivatives of increasing order.

In this paper, we propose a high-resolution approach for detecting magnetic source boundaries. It depends on the application of analytic signal to the horizontal gradient of the magnetic anomaly (or first order horizontal analytic signal), defined as a vector, whose components are the analytic signals of the x- and y-derivatives, respectively. The main idea is that the horizontal gradient of a 3D magnetic body may be considered as the magnetic effect of two thin bodies situated along its extension. Consequently, this will reduce the interference effects and at the same time, the amplitude of the analytic signal of the horizontal gradient, composed of amplitudes of analytic signals computed from the horizontal gradients, will provide an enhanced image and yield a more precise delineation of magnetic bodies.

In order to illustrate the efficiency of this method, we have first given some theoretical examples and compared our results with those obtained by known techniques using both the vertical and the horizontal gradients. Then, the approach was applied to three magnetic anomalies, two, extracted from an Algerian aeromagnetic data set and one from a ground survey. The first is located in the Tin-Seririne basin situated in the south-eastern region of the Hoggar shield (Algeria), the second in the Ougarta range, in the south-western region of the Algerian Sahara, and the third in the Eglab region, in the western region of Algeria.

2. Method

According to Roest *et al.* (1992) the analytic signal of the magnetic anomaly M of a 3D source can be defined as a complex vector

$$AS(x, y) = \frac{\partial M}{\partial x}\hat{x} + \frac{\partial M}{\partial x}\hat{y} + i\frac{\partial M}{\partial z}\hat{z} \qquad (2.1)$$

where i is the complex number and $\hat{x}$, $\hat{y}$ and $\hat{z}$ are the unit vectors in x, y and z directions, respectively.

In the frequency domain eq. (2.1) may be written as follows (Roest *et al.*, 1992):

$$\hat{t} \cdot F[\boldsymbol{AS}(x, y)] = \hat{h} \cdot \nabla F(M) + i\hat{z} \cdot \nabla F(M) . \tag{2.2}$$

The real and imaginary parts of eq. (2.2) being the horizontal and vertical derivatives respectively, form a Hilbert transform pair and are related by the 3D Hilbert transform operator $i(\hat{h} \cdot \boldsymbol{k})/|\boldsymbol{k}|$ as follows:

$$\hat{h} \cdot \nabla F[M] = i \frac{\hat{h} \cdot \boldsymbol{k}}{|\boldsymbol{k}|} \hat{z} \cdot \nabla F[M] \tag{2.3}$$

where $\nabla = ik_x \hat{x} + ik_y \hat{y} + |\boldsymbol{k}| \hat{z}$, represents the gradient operator in the frequency domain, with $\boldsymbol{k} = (k_x, k_y)$ the wavenumber, $\hat{h} = \hat{x} + \hat{y}$ and $\hat{t} = \hat{x} + \hat{y} + \hat{z}$.

The amplitude of the analytic signal is then given by the following formula:

$$|\boldsymbol{AS}(x, y)| = \sqrt{\left(\frac{\partial M}{\partial x}\right)^2 + \left(\frac{\partial M}{\partial y}\right)^2 + \left(\frac{\partial M}{\partial z}\right)^2} . \tag{2.4}$$

For the 2D case, this equation is simplified to

$$|\boldsymbol{AS}(x)| = \sqrt{\left(\frac{\partial M}{\partial x}\right)^2 + \left(\frac{\partial M}{\partial z}\right)^2} . \tag{2.5}$$

Using eq. (2.5) Nabighian (1972) showed that for a thin sheet-like body (dyke), the location of the source in the horizontal plane can be deduced from the positive peaks of the amplitude of the analytic signal and the source depth can be estimated as the half width at half maximum of the amplitude of the analytic signal. Furthermore, the amplitude of the analytic signal over a thin dyke is independent of the angles of inclination and declination of the magnetic field vector and the magnetization vector.

This is not the case when prismatic 3D bodies are encountered, especially if their extents are close enough to produce interference effects and thereby affect the shape of the analytic signal amplitude.

However, the response of the horizontal gradients (x- and y-derivatives) over a thick linear body (2D) is similar in shape to that of two thin isolated bodies situated at its extremities. The first thin body has a magnetization in the direction of the thick body, while the second is in the opposite direction (fig. 1a,b). Below is the demonstration for the case of a 2D thick dyke structure.

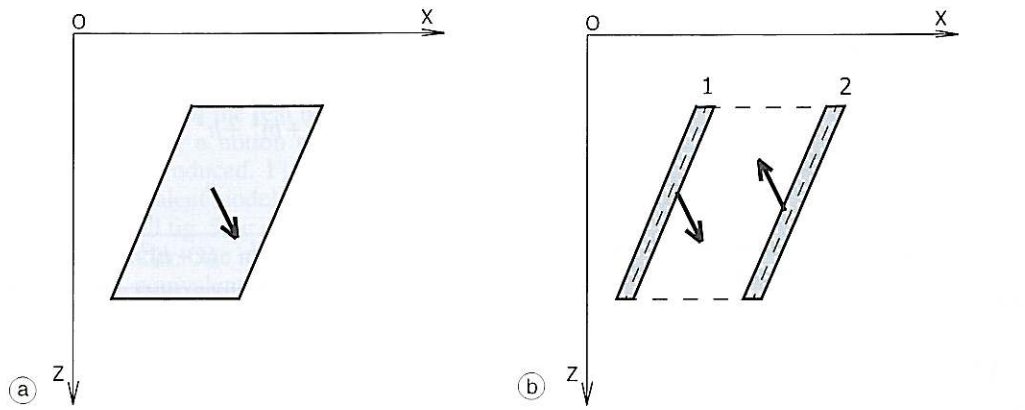

Fig. 1a,b. Equivalent models producing the same magnetic effect and the horizontal gradient effect. a) Cross-sectional view of a 2D model and its corresponding equivalent models 1 and 2 (b). The arrows indicate the magnetization vector orientation.

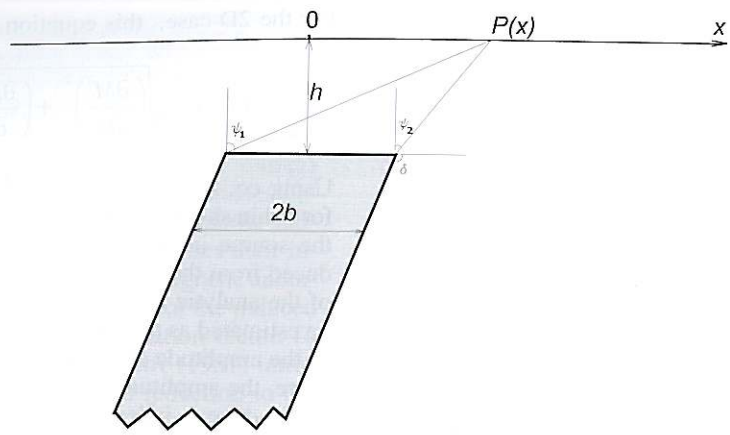

Fig. 2. Cross-sectional view of a 2D model (thick dyke).

The general analytic expression for the magnetic anomaly of total field ΔT in any point $P(x)$ along a perpendicular profile to a thick dyke is given as follows (Rao *et al.*, 1981):

$$\Delta T = A\left[\left(\frac{\psi_1 - \psi_2}{W}\right)\cos\theta + \left(\frac{1}{W}\log_e\frac{\cos\psi_2}{\cos\psi_1}\right)\sin\theta\right] \tag{2.6}$$

where ψ_1 and ψ_2 are the angles as defined in fig. 2.

A – amplitude coefficient;
θ – index parameter;
$W = \frac{2b}{h}$;
$2b$ – dyke width;
h – its depth.

Expressing eq. (2.6) as a function of x (abscissa), h (depth), and b (half width) the following equation can be obtained:

$$\Delta T = A'\left[\left(\tan^{-1}\frac{x+b}{h}\right) - \tan^{-1}\frac{x-b}{h}\right]\cos\theta + \frac{1}{2}\ln\frac{(x+b)+h^2}{(x-b)^2+h^2}\sin\theta \tag{2.7}$$

where:

$A' = \frac{A}{W} = 2kT\sin\delta(1-\cos^2 i\cdot\cos^2\alpha)$;

$\theta = 2I - \delta - 90°$;
k – susceptibility contrast;
T – field intensity;
i – magnetic field inclination;
α – angle formed by the north and the dyke direction;
$I = \arctan(\tan i/\sin\alpha)$;
δ – dip of the dyke.

The horizontal gradient in the x direction of ΔT is deduced following the derivation of eq. (2.7) with regard to the variable x:

$$\Delta T'_x = A'\left\{\left[\frac{x+b}{(x+b)^2+h^2} - \frac{x-b}{(x-b)^2+h^2}\right]\sin\theta - \left[\frac{h}{(x-b)^2+h^2} - \frac{h}{(x+b)^2+h^2}\right]\cos\theta\right\} \tag{2.8}$$

$$\Delta T'_x = A'\left[\frac{(x+b)\sin\theta - h\cos\theta}{(x+b)^2+h^2}\right] - A'\left[\frac{(x-b)\sin\theta - h\cos\theta}{(x-b)^2+h^2}\right] \tag{2.9}$$

denoting $\theta_1 = \theta + 180°$

$$\Delta T'_x = A'\left[\frac{(x+b)\sin\theta - h\cos\theta}{(x+b)^2 + h^2}\right] + \tag{2.10}$$

$$+ A'\left[\frac{(x-b)\sin\theta_1 - h\cos\theta_1}{(x-b)^2 + h^2}\right]$$

$$\Delta T'_x = \Delta T_1 + \Delta T_2 \,. \tag{2.11}$$

Equation (2.11) shows that the horizontal gradient in the x-direction of the magnetic anomaly produced by the thick dyke, is similar to the magnetic effect of two thin dykes where ΔT_1 is the analytic expression for the magnetic anomaly over a thin dyke situated on the left hand-side extremity of the thick dyke and magnetized in the same direction, and ΔT_2 is the analytic expression for the magnetic anomaly over another thin dyke situated on the right hand-side extremity of the thick dyke but magnetized in the opposite direction.

By analogy, it can be demonstrated that the horizontal gradient effect of a prismatic 3D thick body is similar to the magnetic effect of two thin bodies situated at its extremities and perpendicular to the derivation direction, as illustrated in figs. 3a-c, 4a-c and 5a-c. Therefore, the application of an analytic signal to the horizontal gradient provides the same result as if it had been applied to the field anomalies of two thin bodies situated on the flanks of the real body. Because of this, in one sense, a notion of «equivalent models» can be introduced. Figures 3a-c and 4a-c show the equivalent models for simple prismatic structures and fig. 5a-c illustrates the case for a vertical cylinder. One important characteristic is that the equivalent models are either single thin linear bodies or angles (V-shape or L-shape bodies). This characteristic, based on the thin dyke concept, is used in the present study in order to sharpen the analytic signal and to yield an accurate body delineation.

Applying eq. (2.1) to the horizontal gradient instead of the magnetic anomaly, we obtain the following equation for the analytic signal com-

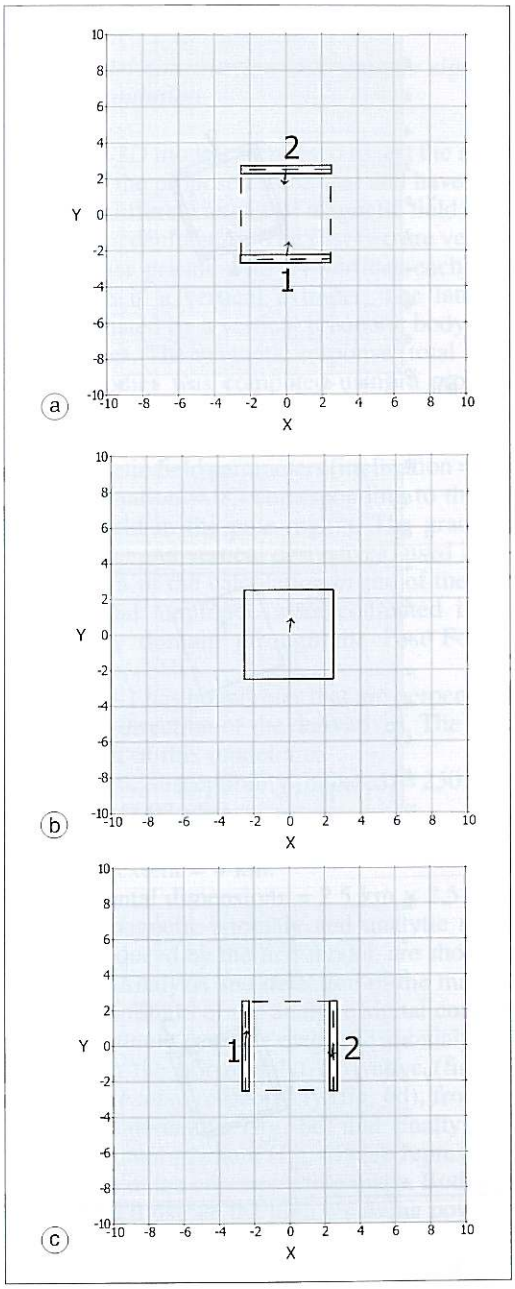

Fig. 3a-c. Plan view of model 1(b) (vertical rectangular prism) and its corresponding equivalent models deduced from x-derivative (c) and y-derivative (a). The arrows indicate the magnetization vector orientation.

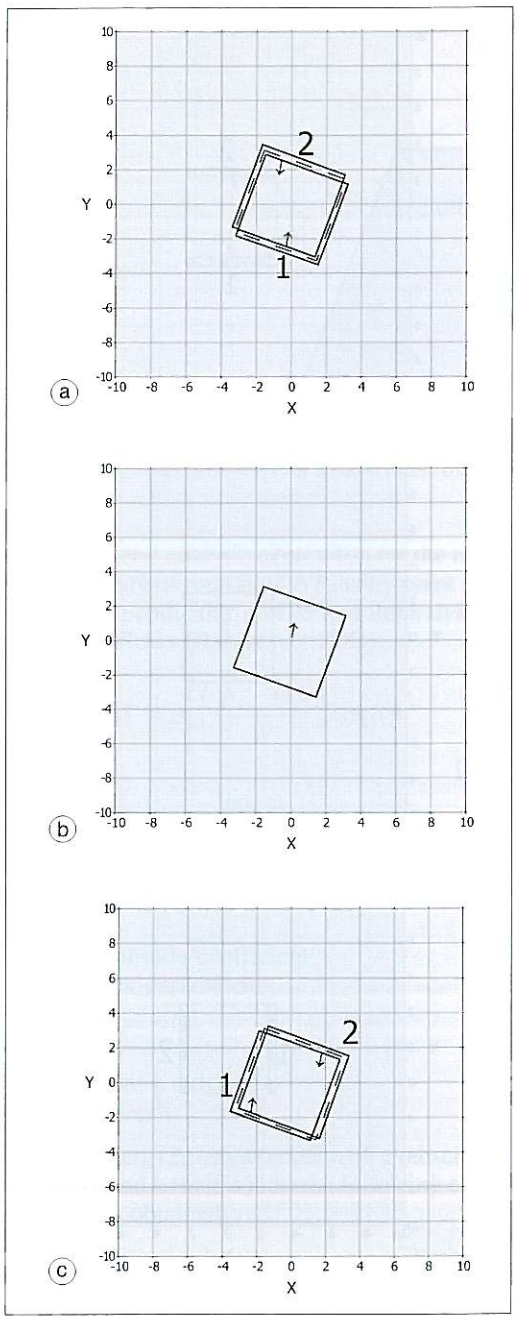

Fig. 4a-c. Plan view of model 2 (b) (vertical prism) and its corresponding equivalent models deduced from x-derivative (c) and y-derivative (a). The arrows indicate the magnetization vector orientation.

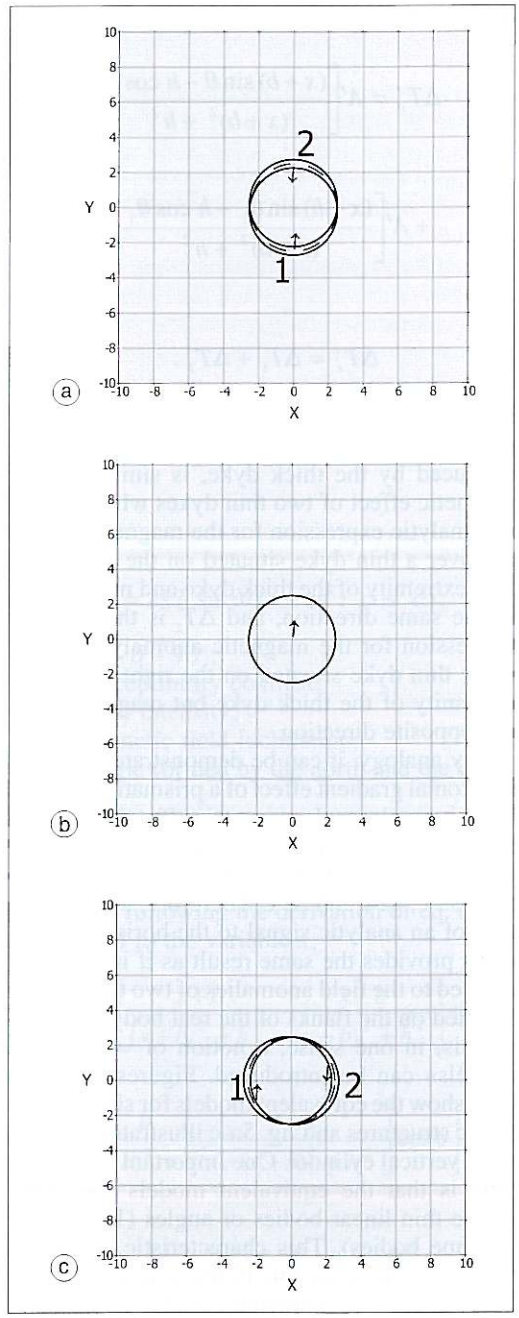

Fig. 5a-c. Plan view of the model 3 (b) (vertical cylinder) and its corresponding equivalent models deduced from x-derivative (c) and y-derivative (a). The arrows indicate the magnetization vector orientation.

puted from the horizontal gradient:

$$\boldsymbol{AS}_h(x,y) = \frac{\partial M_h}{\partial x}\hat{x} + \frac{\partial M_h}{\partial y}\hat{y} - i\frac{\partial M_h}{\partial z}\hat{z} \quad (2.12)$$

where M_h representing the horizontal gradient of M in the h direction, can be decomposed in two orthogonal components as

$$M_h = (M_x, M_y) \quad (2.13)$$

$$\text{where, } M_x = \frac{\partial M}{\partial x} \text{ and } M_y = \frac{\partial M}{\partial y}. \quad (2.14)$$

Regarding to eq. (2.12) the analytic signal amplitudes of the x- and y-horizontal derivatives can be expressed as follows, respectively:

$$\left|\boldsymbol{AS}_x(x,y)\right| = \sqrt{\left(\frac{\partial M_x}{\partial x}\right)^2 + \left(\frac{\partial M_x}{\partial y}\right)^2 + \left(\frac{\partial M_x}{\partial z}\right)^2} \quad (2.15)$$

and

$$\left|\boldsymbol{AS}_y(x,y)\right| = \sqrt{\left(\frac{\partial M_y}{\partial x}\right)^2 + \left(\frac{\partial M_y}{\partial y}\right)^2 + \left(\frac{\partial M_y}{\partial z}\right)^2}. \quad (2.16)$$

The magnitude of the analytic signal of the horizontal gradient is defined here by the following expression:

$$\left|\boldsymbol{AS}_h(x,y)\right| = \sqrt{\left|\boldsymbol{AS}_x(x,y)\right|^2 + \left|\boldsymbol{AS}_y(x,y)\right|^2}. \quad (2.17)$$

As shown hereafter, the expression (2.17) is used in the present work to obtain an accurate delineation of magnetic source boundaries and emphasize their effects. On the other hand, the last expression is similar to the so-called the enhanced horizontal derivative method published by Fedi and Florio (2001).

3. Synthetic models

3.1. *Model construction and analytic signal computation*

Three 3D models were used to test the application of the proposed technique and have been tested at different angles of magnetic field inclination and declination. The first two are vertical rectangular prisms with 04 vertices each. The third one is a vertical cylinder. The latter is approximated by a vertical prismatic body with 36 vertices. The magnetic response (total field) of the bodies was computed using a program based on the methods of Talwani and Heirtzler (1964). The modelling was obtained with the geomagnetic field parameters (inclination = 90°, and declination = 0°) corresponding to the observed field in the pole region. The gradients (horizontal and vertical derivatives) used in the expression of the calculation of the of the analytic signal amplitude were computed in the frequency domain through the Fast Fourier Transform (FFT).

Model 1 has boundaries that are perpendicular to the direction of the derivatives. The characteristics of this model are:

- Magnetic susceptibility (induced) = 250×10^{-5} Cgs (0.0002 uSI).
- Depth to the top = 1 km.
- Depth extent = 4 km.
- Horizontal dimensions = 2.5 km × 2.5 km.

The magnetic anomaly and analytic signal maps produced by the first model are shown in fig. 6a-f. Analysis and detection of the maxima of the amplitude of the analytic signal computed respectively from the magnetic anomaly (fig. 6b), from the horizontal x-derivative (fig. 6c) and y-derivative respectively (fig. 6d), from the z-vertical derivative (fig. 6e) and finally from the horizontal gradient (fig. 6f) are represented by circles in the corresponding maps. Both figs. 6c and 6d illustrate the high resolving power of the analytic signals derived from the horizontal gradients.

It is worth mentioning that the high resolving power in determining southern and northern source boundaries is obtained from the analytic signal of the y-derivative, whereas eastern and western boundaries cannot be clearly defined

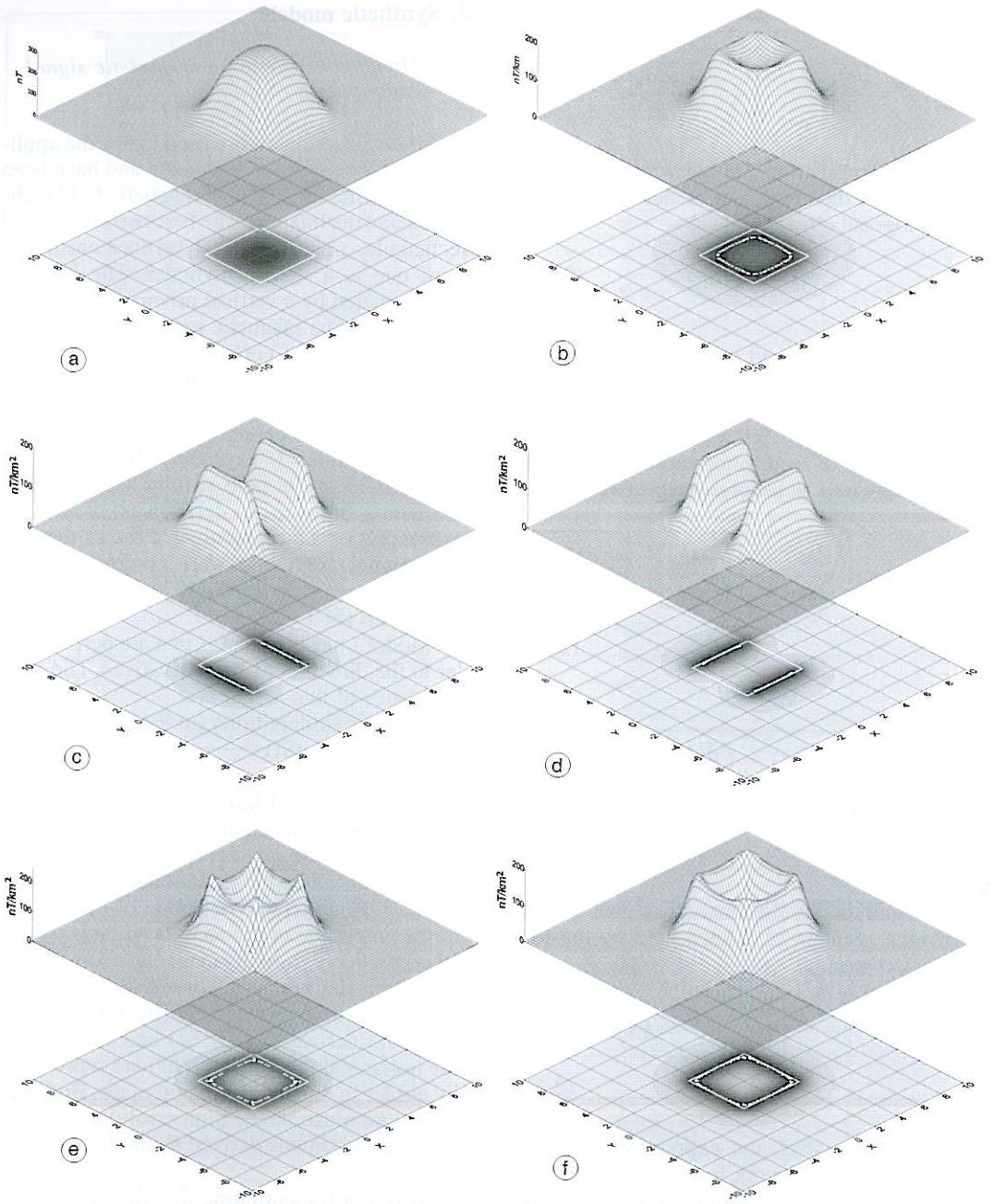

Fig. 6a-f. Magnetic response of model 1. a) Synthetic anomaly (total magnetic field); b) analytic signal of (a); c) analytic signal of the x-horizontal gradient; d) analytic signal of the y-horizontal gradient; e) analytic signal of the vertical gradient; f) horizontal gradient analytic signal. The y-axis indicates the magnetic north and the white rectangle, the source body edges. Determined solutions are indicated by small circles.

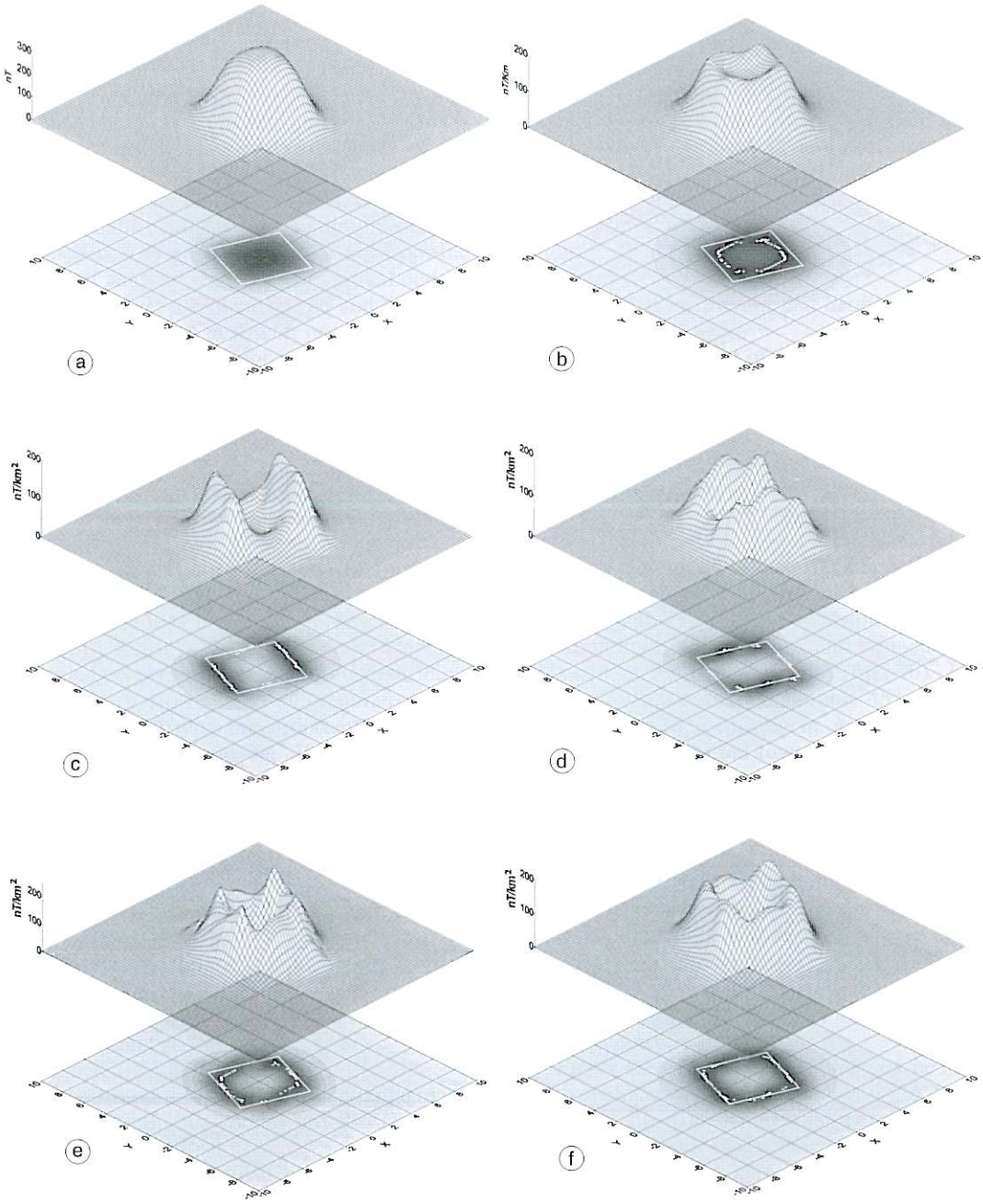

Fig. 7a-f. Magnetic response of model 2. a) Synthetic anomaly (total magnetic field); b) analytic signal of (a); c) analytic signal of the *x*-horizontal gradient; d) analytic signal of the *y*-horizontal gradient, e) analytic signal of the vertical gradient; f) horizontal gradient analytic signal. The *y*-axis indicates the magnetic north and the polygon in solid white line, the source body edges. Determined solutions are indicated by small circles.

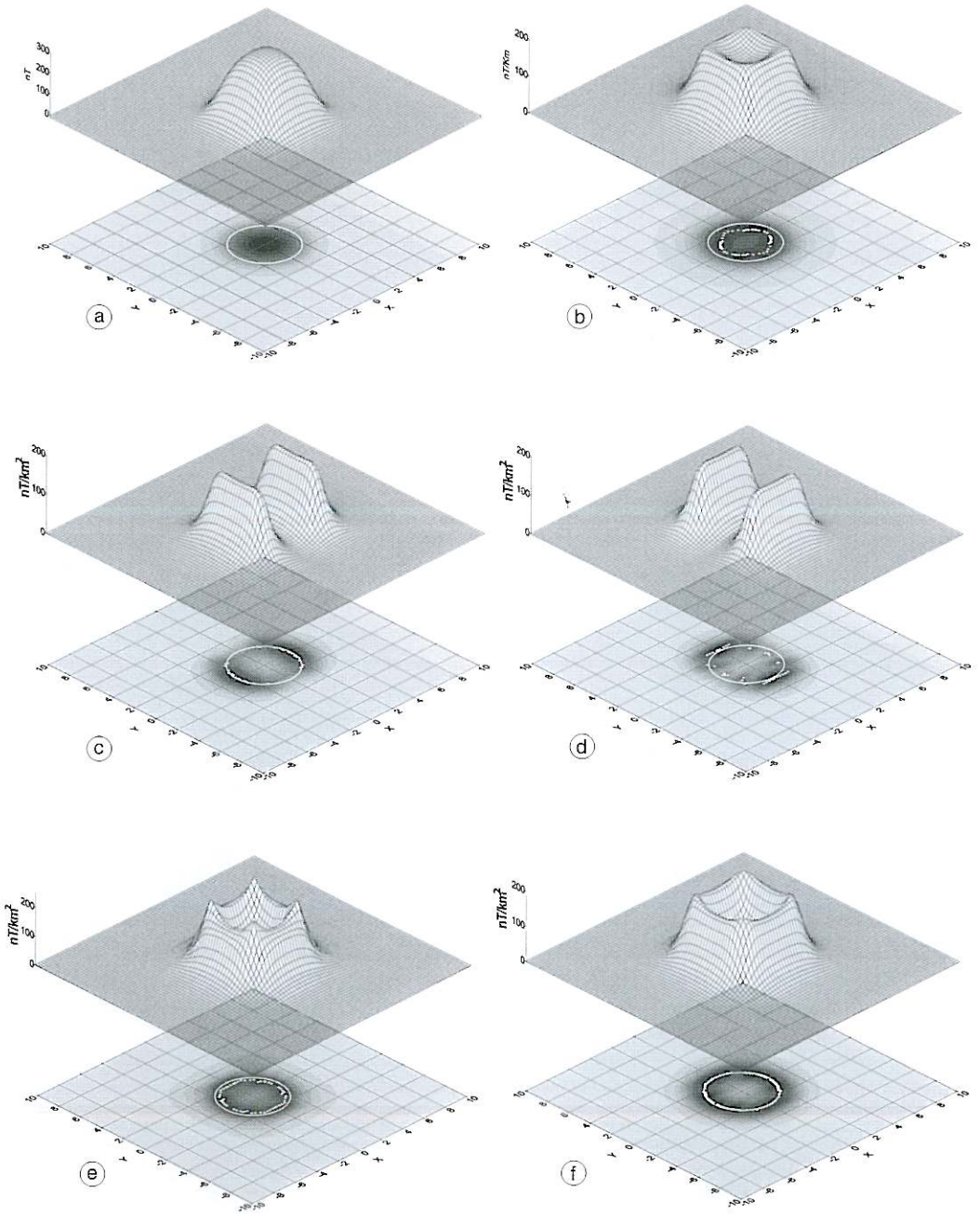

Fig. 8a-f. Magnetic response of model 3. a) Synthetic anomaly (total magnetic field); b) analytic signal of (a); c) analytic signal of the *x*-horizontal gradient; d) analytic signal of the *y*-horizontal gradient; e) analytic signal of the vertical gradient; f) horizontal gradient analytic signal. The *y*-axis indicates the magnetic north. The source body edges are indicated by the circle in solid white line. Determined solutions are indicated by small circles.

by the analytic signal of the x-derivative, but can be represented by the corners of the body. By combining the solutions obtained from the x- and y-derivatives, the proposed analytic signal of the horizontal gradient allows us to exactly delineate the shape and boundaries of the source body (fig. 6f). Figure 6e shows the analytic signal of the vertical gradient. By comparing the results obtained from the simple analytic signal (Roest *et al.*, 1992) in fig. 6b, from the enhanced analytic signal of the vertical derivative (Hsu *et al.*, 1996) in fig. 6e and from the proposed technique in fig. 6f, one can note the similarity in shape but not in amplitude of the analytic signals. However, the highest revolving power in source boundaries detection is obtained from the horizontal gradient analytic signal (fig. 6f).

The characteristics of model 2 are the same as the previous model but its boundaries are not perpendicular to any direction of the derivatives. Figure 7a-f shows the magnetic response produced by model 2. As noticeable, the peaks of the amplitude of the simple analytic signal as defined by Roest *et al.* (1992) do not reflect the source edges correctly and yield a coarse delineation, fig. 7b. However, a more accurate definition is obtained with the proposed horizontal gradient analytic signal, fig. 7f. Here also, one can observe that the analytic signal of the vertical gradient shown in fig. 7e produces a similar shape to that of the analytic signal of the horizontal gradient, but with a less accurate boundary delineation.

Model 3 is a vertical cylinder with the following parameters :

- Magnetic susceptibility (induced) = 500×10^{-5} Cgs (0.0004 uSI).
- Depth to the top = 1 km.
- Depth extent = 4 km.
- Diameter = 5 km.

The magnetic effect and analytic signal maps performed with this model are illustrated in fig. 8a-f.

In this case, the equivalent models are produced by the derivation in both x and y horizontal directions respectively. As shown in figs. 8c and 8d, they have the shape of two opposite arcs. But figs. 8c and 8d show a higher resolving power with the x- and y-horizontal derivatives respectively. Figure 8e shows the analytic signal of the vertical gradient and fig. 8f illustrates the analytic signal of the horizontal gradient. Here also, by comparing the results obtained from known techniques (figs. 8b and 8f) with those obtained with the proposed enhanced approach, it is clear that the latter provides the exact shape of the circular body and yields the most precise body delineation.

3.2. *Effect of inclination and declination*

To study the effect of the magnetization orientation on the final results, computations were performed at various declinations and inclinations of the magnetic field, using model 1.

Figure 9a-e shows the horizontal gradient analytic signal maps at declination = 0° and with various inclination values ranging from a vertical direction (pole) to a horizontal one (equator). The ideal case is when the magnetic inclination is vertical (fig. 9a). All the boundaries are detected with an excellent precision. A less accurate delineation of north-south boundaries is obtained at inclination = 65° (fig. 9b). In a middle latitude case (inclination = 45°, fig. 9c), the determined locations of east-west body boundaries are shifted towards the south with an appearance of secondary maxima to the north of true boundaries. In the case where the inclination is 25° (fig. 9d), the horizontal shift between the true and determined east-west boundaries is minimised but the north-south edges are poorly detected, as in fig. 9c. However, it is worth remarking that in the case of the equator (inclination = 0°) fig. 9e, a very good delineation of the north-south boundaries is obtained, while the east-west boundaries are fairly detected.

Figure 10a-e illustrates the effect of the magnetic declination at fixed inclination (25°). The first case, fig. 10a has already been mentioned above, and since the north-south boundaries are parallel to the magnetic field direction, they are very poorly detected. However, when the magnetic field is not parallel to the model boundaries, these will be detected depending on the angle that the magnetic field makes with either of the boundaries (figs. 10b, 10c and

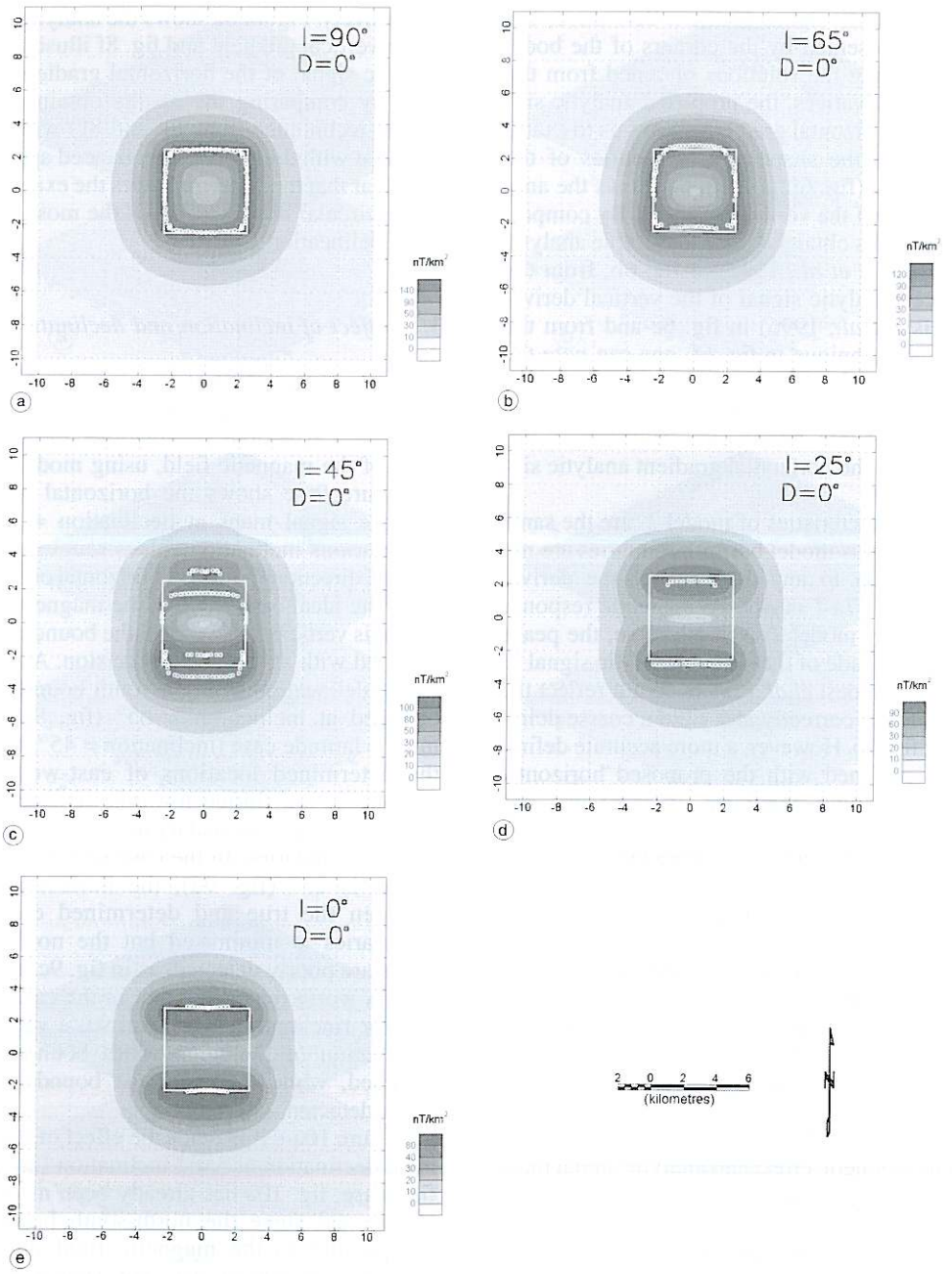

Fig. 9a-e. Amplitude of the horizontal gradient analytic signal of model 1 at fixed magnetic declination ($D = 0°$) and different magnetic inclinations. a) Inclination = 90°; b) inclination = 65°; c) inclination = 45°; d) inclination = 25°; e) inclination = 0°. The white rectangle indicates the source location and circles indicate the determined solutions.

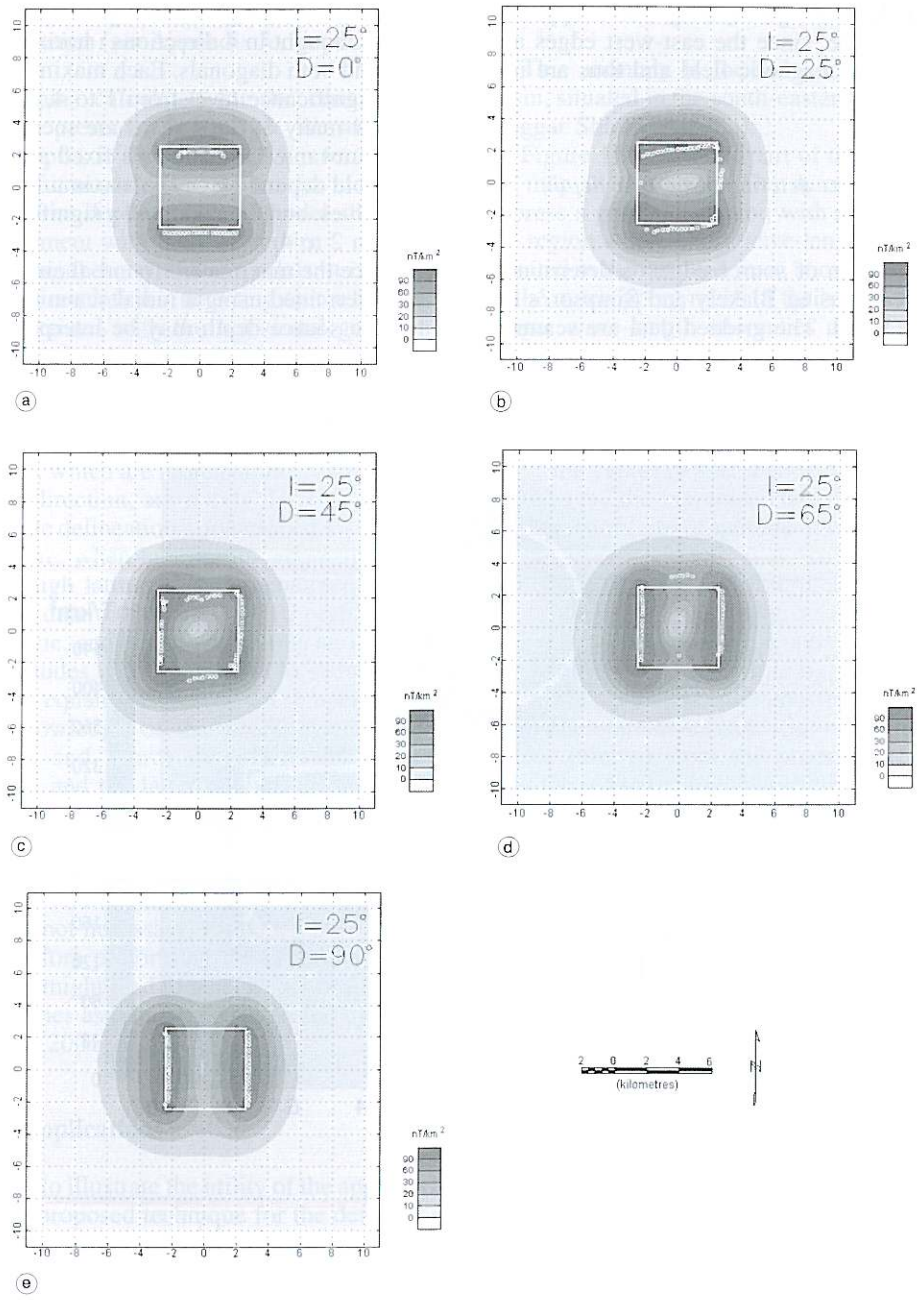

Fig. 10a-e. Amplitude of the horizontal gradient analytic signal of model 1 at a fixed magnetic inclination (I = 25°) and different magnetic declinations. a) Declination = 0°; b) declination = 25°; c) declination = 45°; d) declination = 65°; e) declination = 90°. The white rectangle indicates the source location and circles indicate the determined solutions.

10d). The last case given in fig. 10e is opposite to the first case, since the east-west edges are parallel to the magnetic field and thus are not detected.

3.3. *Boundaries determination and depth estimation*

The location of source edges is determined automatically using Blakely and Simpson's algorithm (1986). The gridded data are scanned by a 3×3 moving window in which a maximum is sought in 4 directions : horizontal, vertical and both diagonals. Each maximum is given a significance level from 1 to 4, depending on how many of the 4 scans are successful. To avoid unwanted maxima, we fixed a minimum threshold depending on the maximum and average values, and then adopted a significance level from 2 to 4.

Once the maxima are found, their directions are determined using a radial scanning method and the source depth may be interpreted from

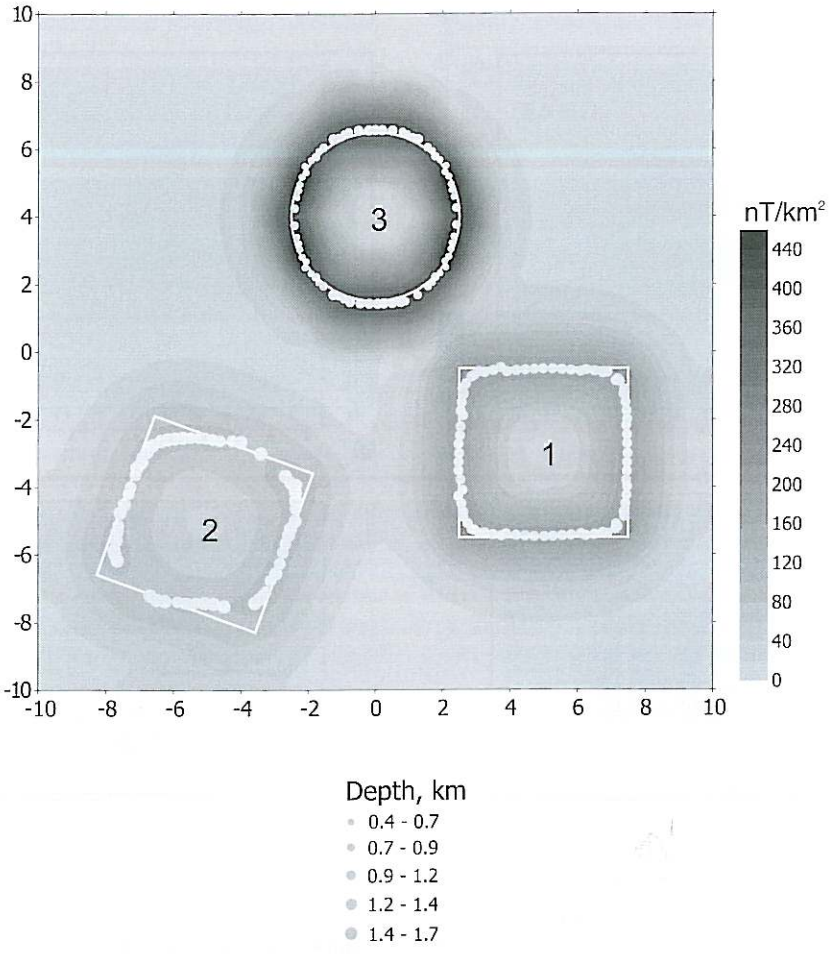

Fig. 11. Source edges determination and depth calculation of the synthetic models situated at different depths: 1 km (1); 1.5 km (2); 0.5 km (3).

the profile crossing the maximum in the perpendicular direction (see Appendix for depth calculation).

The depths calculated for the considered models are presented in fig. 11. We affected different depths to the models: 1 km for model 1, 1.5 km for model 2 and 0.5 km for model 3. The computed depths for each model shows a good agreement with the true depths.

Analysing these synthetic models, it is clear that a higher resolution in detecting source boundaries is obtained with the horizontal gradient analytic signal and a more reliable delineation of source boundaries is obtained for the cases near the pole or the equator. This means that, in the case of the non-vertical magnetization, those boundaries, which are more parallel to the magnetization direction, are poorly detected, and a less accurate delineation is mentioned.

Therefore, when interpreting anomalies observed at high latitudes, it is recommended to reduce the data to the pole before performing the technique, and when interpreting anomalies at low latitudes, it is preferable to reduce the data to the equator. However, these operations require knowledge of the geomagnetic field parameters and source magnetization vector orientation, and the latter may be unknown in the case of remnant magnetization. Furthermore, reduction to the pole at low latitudes needs special care due to the amplification of the effects of the north-south features. But in general, it is useful (but not necessary) to reduce the data to the pole before performing the proposed technique, as it might lead to a better delineation of the boundaries as it has been suggested by Fedi and Florio (2001).

4. Field applications

In order to illustrate the utility of the application of the proposed technique for the determination of the magnetic sources boundaries and their depths, three magnetic anomalies from the southern region of Algeria were treated. Assuming an induced magnetization, the technique was applied to the data with and without reduction to the pole, and then the results obtained for each case were compared.

4.1. *Inazaoua anomaly*

This anomaly is located in the Tinseririne basin, situated in the south-eastern region of the Hoggar Shield (Algeria).

Figure 12 shows one part of the aeromagnetic map of the basin. The aeromagnetic data express a good correlation with the geology of the region where short wave-length anomalies, situated in the east and west, show the signature of the outcropping rocks of the basement, while longer wave-length anomalies dominating the central area reflect the deeper character of the basement. One characteristic of the magnetic field observed in this region is that the inclination is about 25°.

In the centre of the sedimentary basin, one can observe the Inazaoua anomaly, which has a dipolar form. Its amplitude intensity reaches 2000 nT. This anomaly was extracted from the aeromagnetic map and interpreted here using the proposed technique (fig. 13a-d).

Figure 13c shows the results obtained with the observed anomaly, while fig. 13d illustrates the results obtained after the reduction to the pole. The boundaries (fig. 13d) of the magnetic source inferred from the proposed technique after the reduction to the pole are more impressive than those obtained with the data that was not reduced to the pole (fig. 13c). In both cases the interpreted average depth of the body is about 2.5 km.

4.2. *Tabelbala anomaly*

Tabelbala anomaly is located in the southwestern region of the Algerian Sahara.

The aeromagnetic map of this region, fig. 14, shows the existence of short wave-length and high intensity anomalies located at the centre of the map. The main Tabelbala anomaly has an intensity of about 1000 nT. It is surrounded by numerous small and short wave-length anomalies. This anomaly is thought to be a mafic volcanic structure (Paterson *et al.*, 1976).

The Tabelbala anomaly was extracted and interpreted using the analytic signal technique. Figures 15d and 15c illustrate the results ob-

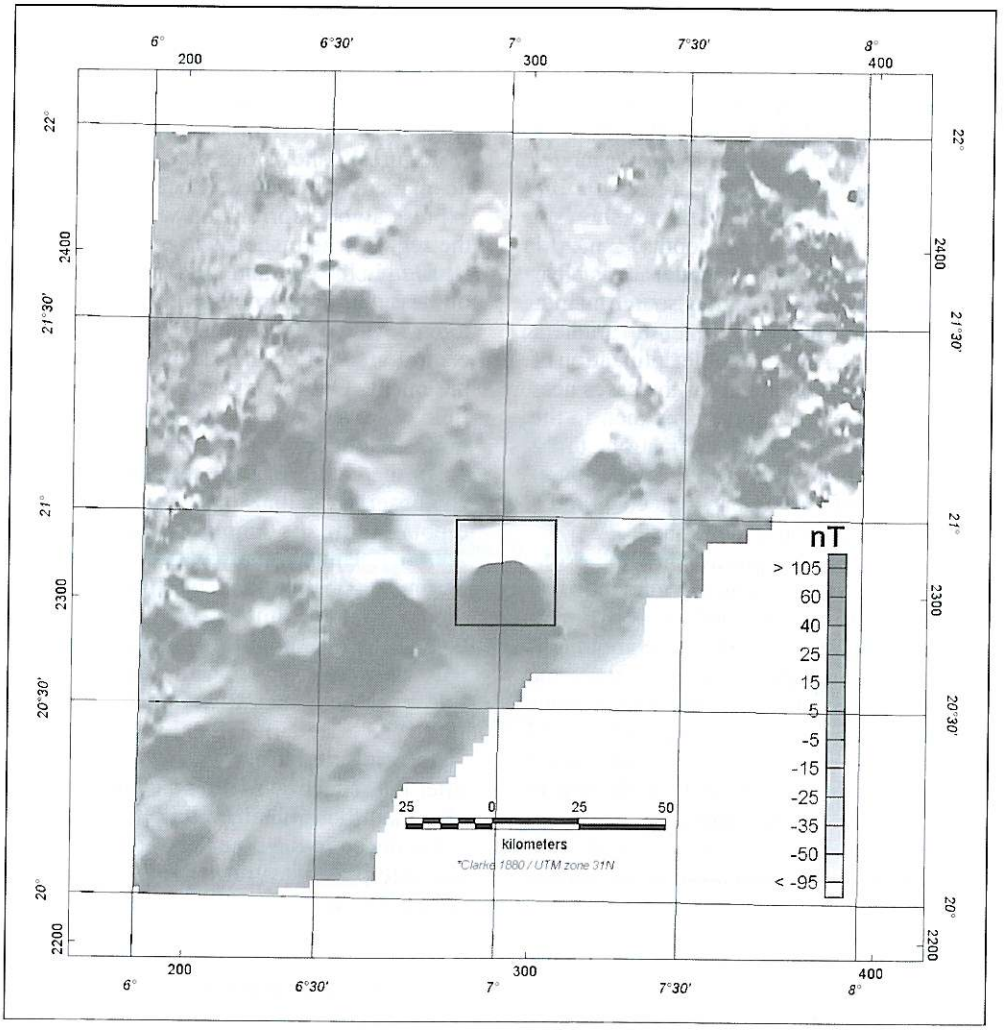

Fig. 12. Aeromagnetic map of the Tinseririne basin. Coordinates are given in degrees and in UTM. The rectangle indicates the Inazaoua anomaly.

tained from the data reduced and unreduced to the pole, respectively.

The results obtained in both cases are slightly different and the interpretation suggests that the source body is composed of two adjacent structures situated at different depths. The first structure is situated at depth between 1 km and 1.25 km while the second is between 1.25 km and 1.5 km.

4.3. *Mdena anomaly*

The ground survey in the Mdena region resulted in a circular magnetic anomaly (fig.16a) that reflects the suspected geological structure. This circular structure is geologically characterised by the presence of volcanic rocks. The center of this structure is at 6°34′ longitude and 26°34′ latitude.

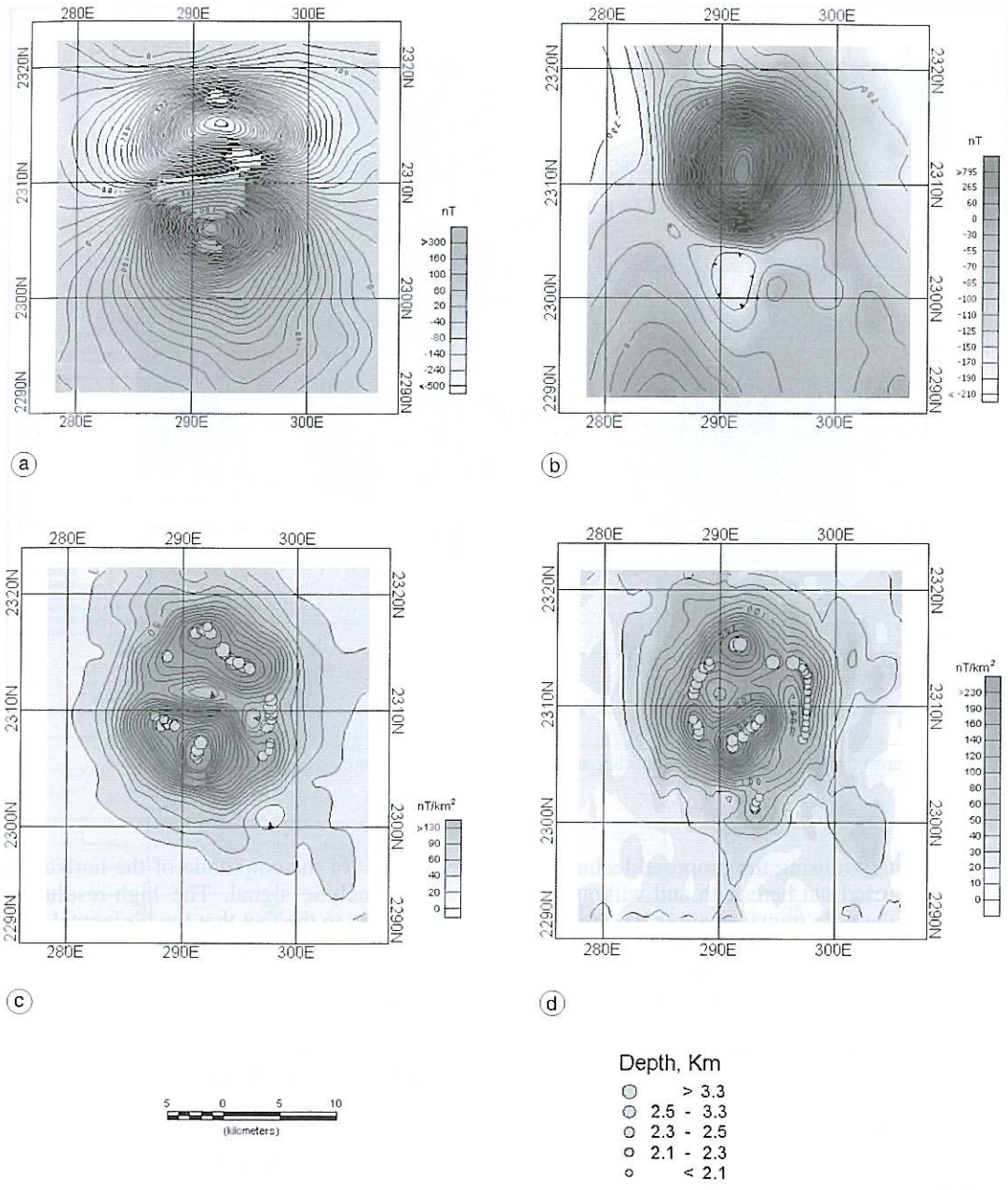

Fig. 13a-d. a) Inazaoua anomaly (base level removed) extracted from the map of fig. 11; b) anomaly (a) reduced to the pole; c) horizontal gradient analytic signal of the anomaly; d) horizontal gradient analytic signal of the anomaly reduced to the pole. The source body boundaries inferred from the proposed technique are indicated by circles.

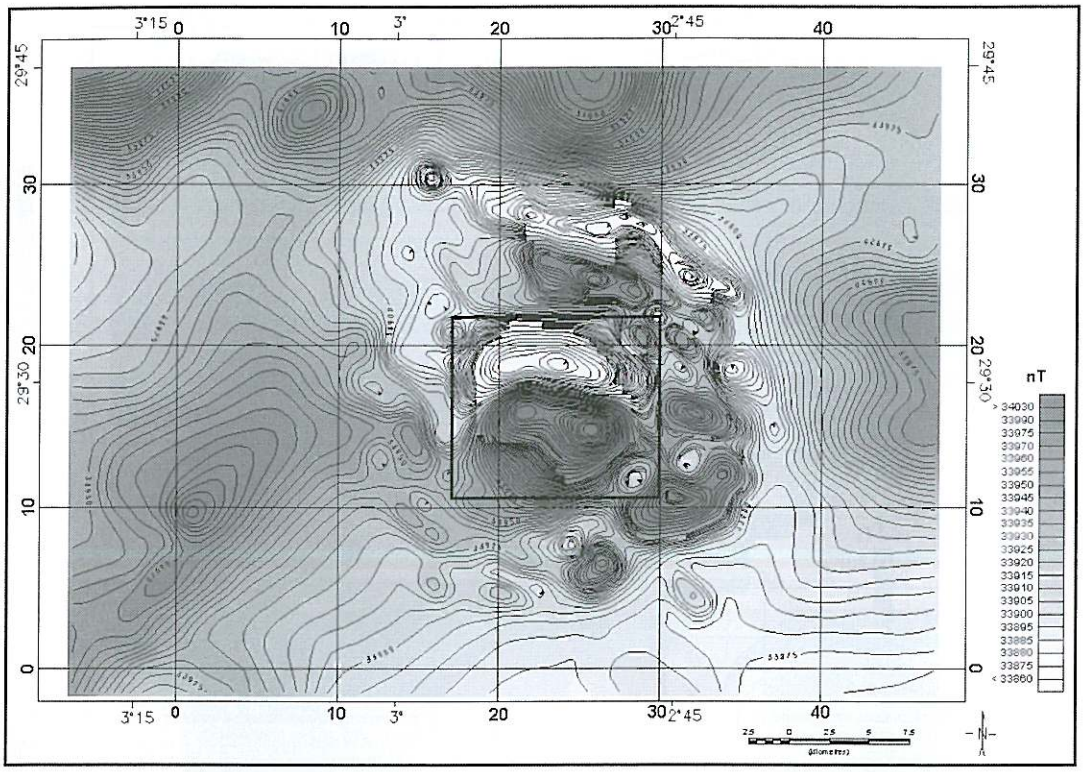

Fig. 14. Aeromagnetic map of the Tabelbala area. The rectangle indicates the Tabelbala anomaly.

Interpretation using the proposed technique was also carried out here with and without reduction to the pole transformation. The results given in fig.16c, obtained with the data not reduced to the pole, do not differ greatly with those obtained with the data reduced to the pole, fig.16d. The calculated depths of the causative structure vary between 125 m and 175 m.

5. Conclusions

The analytic signal of the horizontal gradient derived from the horizontal gradients in both the x- and y-directions of the magnetic anomalies provides an accurate detection of the horizontal extents of source bodies. The source boundaries can be determined by the location of the maxima of the amplitude of the horizontal gradient analytic signal. The high-resolution power is due to the fact that the horizontal gradient emphasizes the source edges effects, reduces the interference effects of the anomalies and yields an enhanced image of the boundaries.

The results obtained from three synthetic models have shown that the source boundary locations are more precisely determined compared to those obtained with other known techniques which use the magnetic anomaly or its vertical derivative.

We have found that a more reliable interpretation is obtained for vertical magnetization than for the tilted one. Good results were also obtained for the equator case, but the boundaries more parallel to the magnetic field orientation

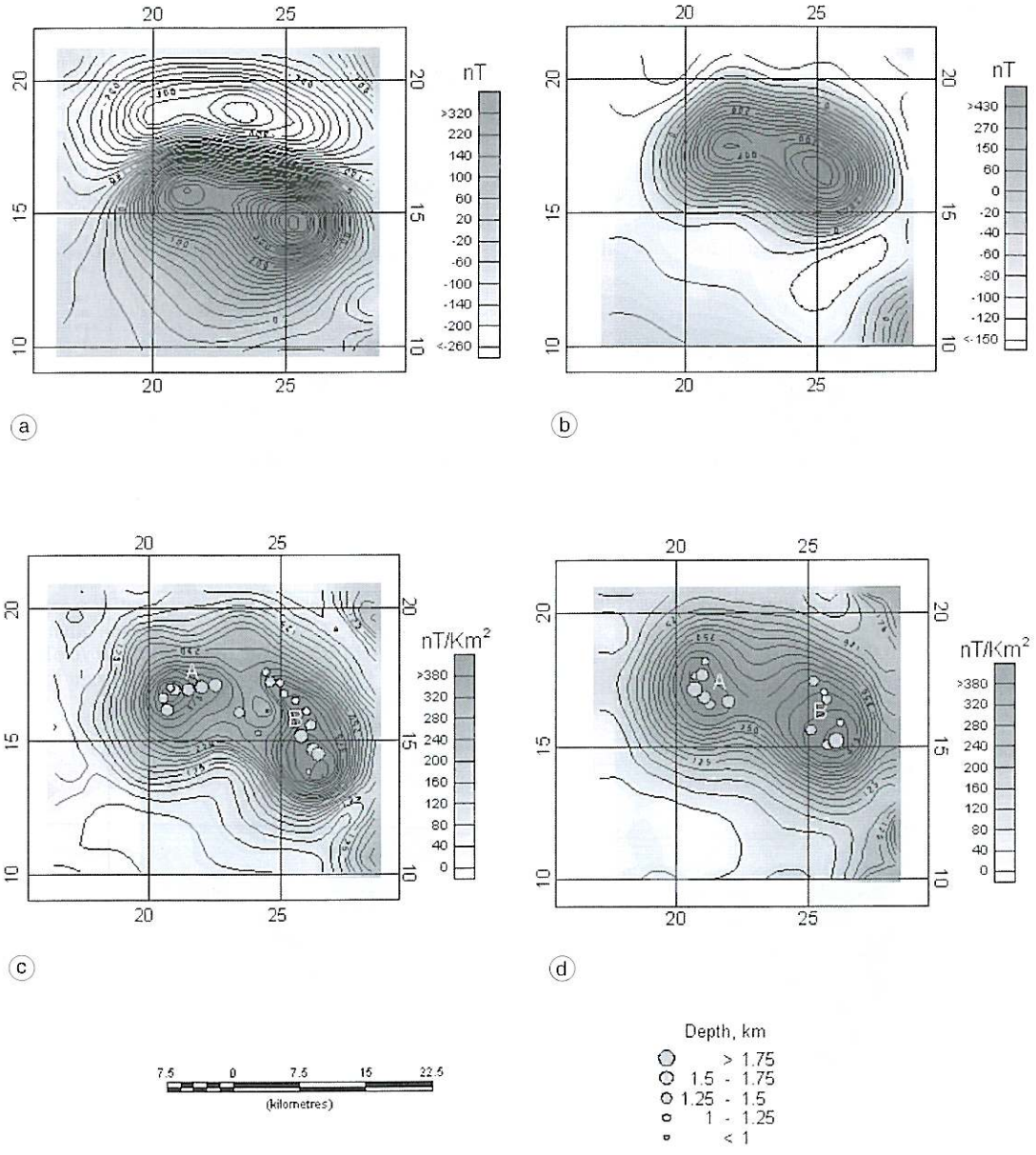

Fig. 15a-d. a) Tabelbala anomaly (with regional trend removed) extracted from the map of fig. 14. b) Anomaly (a) reduced to the pole; c) horizontal gradient analytic signal of (a); d) horizontal gradient analytic signal of (b). The source body boundaries inferred from the proposed technique are indicated by circles.

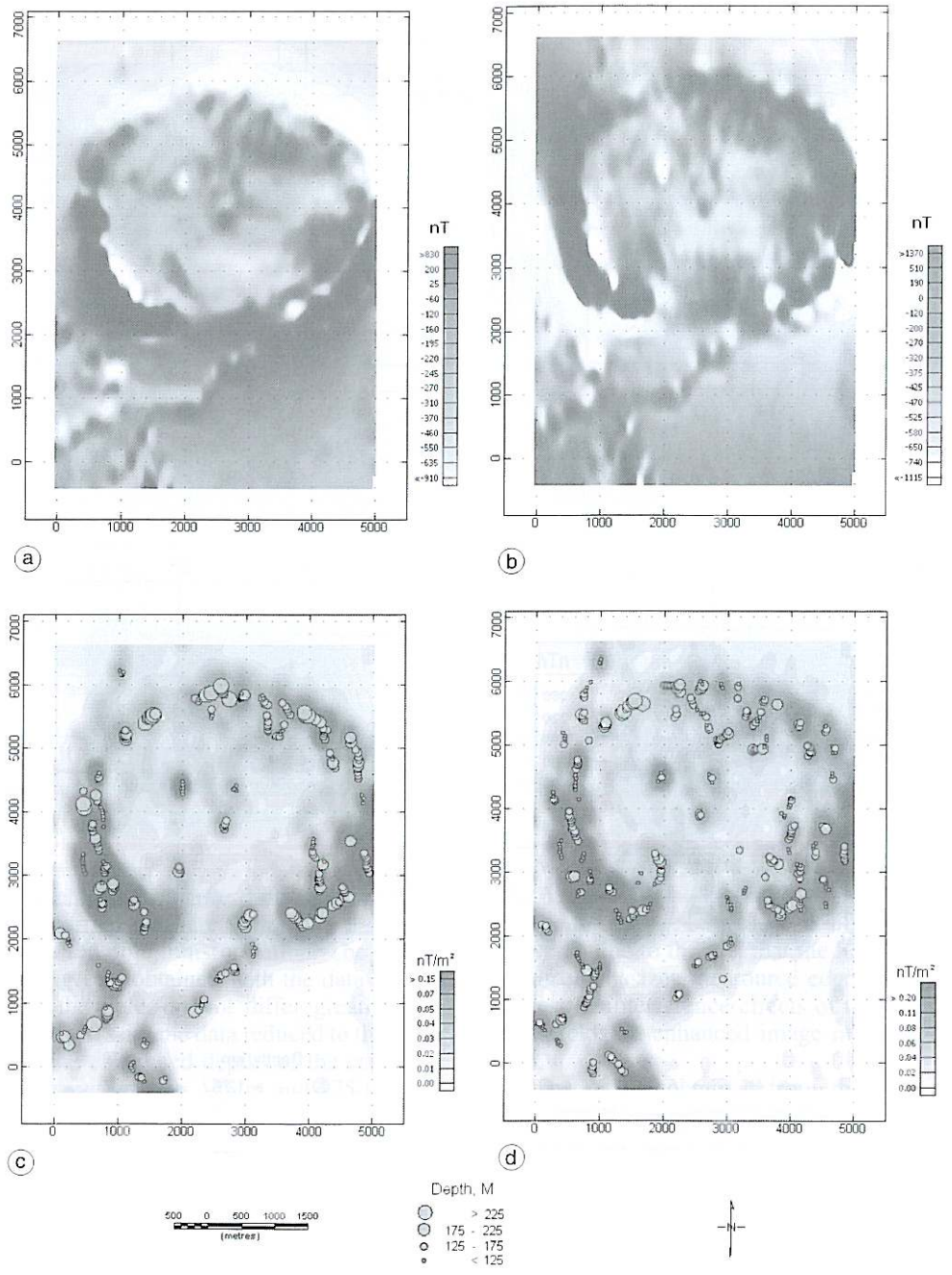

Fig. 16a-d. a) Mdena anomaly extracted from a ground survey; b) anomaly (a) reduced to the pole; c) analytic signal of the horizontal gradient of (a); d,c) analytic signal of the horizontal gradient of (b). The circles indicate the source body coordinates inferred from the proposed technique.

are weakly determined. To obtain more precision of source body outlines and to avoid problems with the magnetic field inclination, it is therefore recommended to reduce the data to the pole before performing the interpretation process. This technique has been successfully applied to synthetic models featuring most of the 3D geological structures. It is also used in the interpretation of three anomalies observed in the south of Algeria (low latitude case). Consequently, this method can be used as an efficient tool for the accurate interpretation of magnetic anomalies.

Acknowledgements

The authors are grateful to Dr. M. Fedi, for his very useful and constructive comments, which have significantly improved the quality and the scope of this work.

Appendix. Depth calculation.

The source depth h may be deduced from the half-width at half-maximum of the amplitude of the horizontal gradient analytic signal, as shown in fig. A.1, using the following equation for the analytic signal of a thin dyke (Nabighian, 1972).

$$|AS(x)| = |\alpha| \frac{1}{(h^2 + x^2)} . \qquad (A.1)$$

Where α is the index parameter depending on the geomagnetic field parameters, magnetization and the dip of the magnetic source.

To avoid interference effects and to obtain a more reliable depth estimation, we computed the source depth at 0.8 of maximum of the amplitude of the signal (fig. A.2).

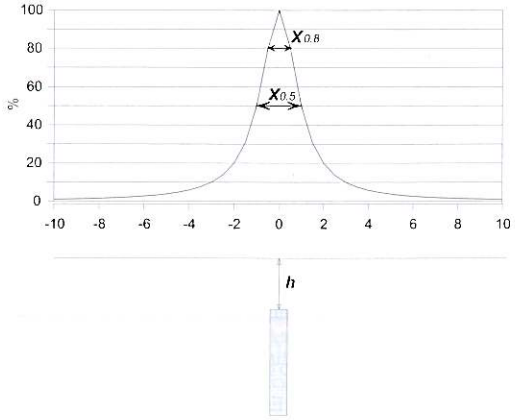

Fig. A.1. This figure shows the amplitude of the analytic signal over a thin dyke and the corresponding distances at half-maximum and at 0.8 maximum, used for apparent depth computation.

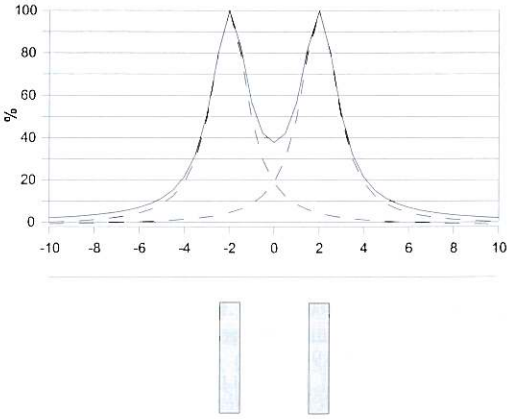

Fig. A.2. Shows the interference effects of the analytic signal curves caused by nearby located dykes. Note that the depth computation at half-maximum is over-estimated.

At maximum (x = 0), the amplitude of the analytic signal, is directly related to the depth by the simple following expression:

$$|AS(x)|_{max} = |\alpha| \frac{1}{h^2} . \quad (A.2)$$

At 0.8 value of maximum, relation (A.1) will be written as follows:

$$|AS(x_1)| = |\alpha| \frac{1}{(h^2 + x_1^2)} \quad (A.3)$$

or

$$|AS(x_1)| = 0.8 \cdot |AS(x)|_{max} \quad (A.4)$$

where x_1 is the abscissa corresponding to the value of 0.8 maximum.

Replacing both members of eq. (A.4) by their corresponding values in (A.1) and (A.2), we obtain the following equation:

$$h^2 = 4 \cdot x_1^2 . \quad (A.5)$$

Solving eq. (A.5) for x_1, we obtain the following values for the roots ($x_1 = h/2$ *and* $x_1' = -h/2$).

Finally the depth h is estimated using the distance between the abscisses x_1 *and* x_1', *denoted* by $x_{0.8}$ (the width of the maximum at 0.8 of its value):

$$h = x_{0.8} \quad (A.6)$$

REFERENCES

BARANOV, V. (1957): A new method for interpretation aeromagnetic maps: pseudo-gravimetric anomalies, *Geophysics*, **22**, 359-383.

BLAKELY, R.J. and R.W. SIMPSON (1986): Approximating edges of source bodies from magnetic or gravity anomalies, *Geophysics*, **51**, 1494-1498.

CORDELL, L. and V.J.S. GRAUCH (1985): Mapping basement magnetization zones from aeromagnetic data in the san Juan basin, New Mexico, in *The Utility of Regional Gravity and Magnetic Anomaly Maps*, edited by W.J. HINZE, Soc. Expl. Geophys., 181-197.

DEBEGLIA, N. and J. CORPEL (1997): Automatic 3D interpretation of potential field data using analytic signal derivatives , *Geophysics*, **62**, 87-96.

FEDI, M. and G. FLORIO (2001): Detection of potential fields source boundaries by enhanced horizontal derivative method, *Geophys. Prospect.*, **49**, 40-58.

HSU, S.-K., J.-C.SIBUET and C.-T. SHYU (1996): High resolution detection of geologic boundaries from potential-field anomalies: an enhanced analytic signal technique, *Geophysics*, **61**, 373-386.

HSU, S.-K., D. COPPENS and C.-T. SHYU (1998): Depth to magnetic source using the generalized analytic signal, *Geophysics*, **63**, 1947-1957.

MARSON, I. and E.E. KLINGELE (1993): Advantages of using the vertical gradient of gravity for 3D interpretation, *Geophysics*, **58**, 1588-1595.

NABIGHIAN, M.N. (1972): The analytic signal of two-dimentional magnetic bodies with polygonal cross-section: its properties and use for automated anomaly interpretation, *Geophysics*, **37**, 507-517.

NABIGHIAN, M.N. (1974): Additional comments on the analytic signal of two dimensional magnetic bodies with polygonal cross-section, *Geophysics*, **39**, 85-92.

NABIGHIAN, M.N. (1984): Toward a three-dimensional automatic interpretation of potential field data via generalized Hilbert transforms: fundamental relations, *Geophysics*, **49**, 780-786.

PATERSON, GRANT and WATSON, LTD (1976): Réinterprétation des levés aéro-magnéto-spectrométriques de l'Algérie.

RAO, A.D., H.V. RAM BABU and P.V. SANKER NARAYAN (1981): Interpretation of magnetic anomalies due to dikes: the complex gradient method, *Geophysics*, **46**, 1572-1578.

REID, A.B., J.M. ALLSOP, H. GRANSER, A.J. MILLETT and I.W. SOMERTON (1990): Magnetic interpretation in three dimensions using Euler deconvolution, *Geophysics*, **55**, 80-91.

ROEST, W.R., J. VERHOEF and M. PILKINGTON (1992): Magnetic interpretation using the 3D analytic signal, *Geophysics*, **57**, 116-125.

SPECTOR, A. and F.S. GRANT (1970): Statistical models for interpretation aeromagnetic data, *Geophysics*, **22**, 359-383.

TALWANI, M. and J.R. HEIRTZLER (1964): Computation of magnetic anomalies caused by two-dimensional bodies of two-arbitrary shape, in *Computers in the Mineral Industries, Part 1*, edited by G.A. PARKS, *Stanford Univ. Publ., Geolog. Sci.*, **9**, 464-480.

THOMPSON, D.T. (1982): EULDPH: a new technique for making computer-assisted depth estimates from magnetic data, *Geophysics*, **47**, 31-37.

(received July 15, 2000;
accepted June 26, 2001)